2.

Conf-9406201--1

4th European Vacuum Conf. & 1st Swedish Vacuum Meeting, Uppsala, Sweden, 6/13-17/94.

BNL-49809

DEVELOPMENTS IN THE VACUUM SYSTEMS OF AGS-RHIC*

H.C. Hseuh and K.M. Welch

Brookhaven National Laboratory
Upton, New York 11973-5000 USA

Abstract

The Alternating Gradient Synchrotron (AGS) is a synchrotron for the acceleration of protons and heavy ions to tens of GeV/amu for fixed target physics research. The Relativistic Heavy Ion Collider (RHIC), with the AGS as its injector, allows the collision of heavy ion beams with energies of several hundred GeV/amu. The vacuum systems of the AGS-RHIC complex range from 10^{-6} Torr in the ion sources to ultrahigh vacuum of low 10^{-11} Torr in the Booster and RHIC. The status of the machines will be described with emphasis on the following areas: the performance of the Booster ultrahigh vacuum system, the development of non-magnetic vacuum components for the muon storage ring, and progress in the construction of the RHIC vacuum systems.

1. Introduction

A schematic layout of the AGS-RHIC facility is shown in Fig. 1. It consists of the proton Linac, the 16 MV Tandem van deGraff, the Booster synchrotron and the AGS. A muon storage ring with a circumference of 45 m and RHIC with a circumference of 3.8 km are presently under construction. Some of the machine parameters of these accelerators and storage rings are described below.

The Linac accelerates protons to 200 MeV. The Tandem Van de Graaff accelerates heavy ions ranging from oxygen at 8 MeV/amu to gold at 1 MeV/amu. The Booster synchrotron was

*Work performed under the auspices of the U.S. Department of Energy.

commissioned in 1991.[1] It accelerates the protons from the Linac to 1.5 GeV and all ranges of ion beams from the Tandem to several hundred MeV/amu. The AGS accelerates the 1.5 GeV protons from the Booster to 28 GeV. The fully stripped light ions from the Booster, such as O^{+8}, Si^{+14}, are accelerated in the AGS to 14.6 GeV/amu. The partially stripped heavy ions from the Booster, such as Au^{+14} and Au^{+33}, are stripped by a copper stripping foil to Au^{+77} before being injected into the AGS for acceleration to over 10 GeV/amu. At the moment, both protons and heavy ions are extracted from the AGS for fixed target experiments. The AGS will serve as an injector for RHIC.

The objective of the muon storage ring is to measure the magnetic moment of the muons with a precision of 0.3 ppm.[2] Muons, produced by bombarding an external target with 24 GeV protons from the AGS, are stored using a continuous superconducting magnet, $\sim$15 m in diameter. To achieve the precision of 0.3 ppm, the magnetic field uniformity around the muon storage region must be within 1 ppm. This rules out the use of materials with magnetic susceptibilities greater than 10^{-4} near the storage region.

The objective of RHIC is to do physics research involving the collisions of highly relativistic particle beams. The RHIC machine, described elsewhere,[3] must store two counter-rotating particle beams for periods of greater than 10 h. Colliding beams may comprise protons, gold ions (i.e., Au^{+79}), or a variety of heavy ions, colliding with each other or protons.

The vacuum systems of the Linac, Tandem and AGS are of the conventional types operated in high vacuum ranges. Ultrahigh vacuum is needed in the Booster and RHIC to minimize the beam loss due to the interaction of the heavy ions with residual gas molecules. The design and development of these two ultrahigh vacuum systems will be presented in this article. The development of non-magnetic distributed ion pumps and cold cathode gauges for the muon storage ring will also be described.

2. The Booster Vacuum System

The Booster ring has a circumference of 202 m. Details of the Booster vacuum system

are described elsewhere.[4] To achieve the required vacuum of low 10^{-11} Torr, the entire vacuum system is insitu baked to 250°C and is pumped by titanium sublimation pumps and sputter-ion pumps with a total pumping speed over 50,000 ℓ/sec. After the Booster's commissioning in 1991, pressure in over half of the ring was in the 10^{-12} Torr range, which is beyond the measuring limit of Booster's thin collector Bayard-Alpert gauges (BAGs).[5] Pressures at a few kicker magnets remain at low 10^{-10} Torr range, resulting in an average ring vacuum of low 10^{-11} Torr.

Ultrahigh vacuum is usually not required for accelerators. However, the Booster has to accelerate partially stripped, low energy heavy ions, such as Au^{+14} injected at 1 MeV/amu from the Tandem. These ions will exchange electrons with the residual gas molecules with significant cross sections, which causes their immediate loss in the bending magnets. The intensity in time of a Au^{+33} beam during the Booster acceleration cycle was measured at two different vacuum levels. The results are summarized in Fig. 2 and compared with the calculated survival rates using the empirical formula outlined in ref. 6 and the partial pressures measured with residual gas analyzers. At a pressure of 10^{-9} Torr, comprising 50% Ar, 30% CH_4, 15% H_2 and 5% CO, and achieved by turning off all the ring ion pumps, the beam intensities in time are consistent with the calculated values. At the normal operating pressure of $3x10^{-11}$ Torr with 70% H_2, 20% CO, 5% CO_2 and 5% CH_4, beam loss is higher than predicted. This may be caused by non-vacuum related phenomena. The charge exchange cross sections[6] will be higher for Au^{+14}, for which vacuum-related beam loss at $3x10^{-11}$ Torr is estimated to be over 40% during the Booster acceleration cycles.

At a pressure of 10^{-11} Torr, the collector current of the BAGs is only a few pA. This current is transmitted by fully shielded, low dielectric, low noise coaxial cables to the gauge controllers.[5] Some of these gauge cables have lengths of up to 150 meters. During Booster operation, oscillations in some BAG readouts were observed to range from 10^{-12} Torr to low 10^{-9} Torr equivalent. Two major sources of interference have been identified: (1) the EMI due to

the fast pulsing magnets; and, (2) triboelectric current due to the movement of the cables in the outdoor cable trays. The magnitude of the EMI noise pickup is proportional to $\delta B/\delta t$, the ramping rate of the magnetic field.[5] The effect of this bipolar, low frequency noise pickup can be minimized by lengthening the integration intervals of the gauge controllers to a few seconds. The magnitude of the triboelectric current, as shown in Fig. 3, is consistent with both the outdoor length of the cables and the solar radiation intensity. We are investigating the use of low triboelectric cables or relocating the cables to indoor cable trays.

3. The Muon Storage Ring Vacuum System

A pressure of 10^{-8} Torr is required for the muon storage ring. This level of vacuum is not difficult to achieve in conventional accelerators and storage rings. However the need to maintain the magnetic field uniformity at the storage region to within $\pm$ 1 ppm has excluded the use of material, with magnetic susceptibilities greater than 10^{-4}, such as stainless steel and inconel, around the storage region. The chambers are fabricated out of aluminum. Other components will be made of aluminum, brass, ceramic and polymers. Distributed ion pumps (DIPs) will be used to pump the beam vacuum. Both cathodes and anodes of the DIPs will be constructed of titanium. The fringe field of the storage ring magnet at the DIP location ranges from 12 to 15 kilogauss and with direction from vertical plane up to 9°.

To optimize the design of DIPs, the pumping behavior of ion pump elements of different anode radii has been studied using an electromagnet. As shown in Fig. 4, the pumping speeds of the elements with large cell radii decrease with increasing magnetic field while those of smaller cells remain relatively constant. The measured speeds of the smaller cells are consistent with the calculated values[7] using the empirical formula of Suetsugu and Nakagawa.[8] When the direction of the magnetic field is not parallel with the anode axis, the effective cell radius and, therefore, the pumping speed decreases.[9] The dependence of the pumping speeds on the alignment angle for the element with a cell radius of 5.5 mm is shown in Fig. 5, and is compared with that of an element with a cell radius of 9 mm. At a field greater than 10 KG, the

pumping speeds of the smaller cells are found to be more sensitive to misalignment than those with the larger cells.

The storage ring vacuum will be monitored by cold cathode gauges when the DIPs are *not* powered. Several cold cathode gauges, with their permanent magnets removed, have been studied for their suitability when operating in the fringing magnetic field of the storage ring.[10] The discharge intensities of both a grounded Penning gauge and an inverted magnetron gauge decrease with increasing magnetic field and with misalignment to the field. However, at a high magnetic field, the discharge intensities of a Penning gauge, as shown in Fig. 6, increase with a larger misalignment. This observation, first reported by Welch in 1972,[11] is not consistent with our understanding of the Penning discharges and will be the subject of further studies.

4. The RHIC Vacuum Systems

In RHIC, the intensity, and thus the usefulness, of the particle beams is diminished when the stored particles are lost from their contrived orbits either due to charge exchange processes or through nuclear scattering with background gas. Particle beam collisions with gas in regions near the experimental detectors will also cause background noise in these detectors, and are therefore undesirable. For these reasons, a low operating pressure in the RHIC is very important. The RHIC, illustrated in Fig. 7, comprises two interweaving rings $\sim$3.8 km in circumference. About 17% of the life of each beam is spent in warm, room temperature (RT) sections of the rings; the remainder is spent in beam pipe operating at a temperature of $\sim$4.2°K (i.e., the cold bore). An average pressure of $\leq 5\times10^{-10}$ Torr is required in the warm sections, comprising 90% H_2, 5% CO, and 5% CH_4. The requirement for the average total pressure of the cold bore is $\leq 10^{-11}$ Torr, comprising exclusively He and H_2, since all other gases have vapor pressures far below 10^{-11} Torr at 4.2°K. Maintenance of the above pressures assure adequate beam lifetimes and acceptable beam-emittance growth rates.

Figure 8 is a schematic representation of one twelfth of the machine. We see from this figure that RHIC actually comprises three vacuum systems: (1) the cold-bore system; (2) the

warm-bore system; and, (3) the cryostat vacuum system housing the superconducting magnets. Each will be briefly discussed.

Figure 9 provides a graphical representation of a "string" of dipole and CQS (corrector/quadrupole/sextupole) magnets. Magnet helium interconnects are not shown in this figure. The upper portion of this figure shows the magnets with interconnecting beam pipes and vacuum apparatus, whereas the lower portion shows this equipment housed in the magnet cryostats. Beam position monitors subtend each CQS magnet. At alternate locations either sorption pumps or gauge conduits are attached to the cold-bore beam pipe every 30 m.

It was thought prudent in the construction of the RHIC machine to require that no welded, brazed, or bolted vacuum joints serve as barriers between the cryogenic helium (LHe) and ultrahigh vacuum (UHV) environments. This is because LHe leak has a factor of $\sim 10^{+2}$ greater leak rate than an equivalent RT gaseous He leak. Helium cryogen, separately plumbed from one magnet to the next, is pumped through holes in the stacked laminations of the various superconducting magnets. Welded stainless steel shells, containing and aligning the magnet laminations serve as LHe barriers from the cryostat insulation vacuum. The cold bore beam pipe comprised a seamless, austenitic stainless steel tube, extending beyond the end plates of the magnets to which it is welded. The cold bore is interconnected between magnets with formed bellows. Therefore, the only means whereby He can leak into the cold-bore UHV system is through metallurgical flaws in the seamless pipe, because of possible damage caused during the welding of the beam pipe to the magnet end plates, or from the circumstance of gaseous He in the cryostat leaking through a catastrophic failure in the UHV interconnecting piping or bellows.

The sorption pumps, located at 30 m intervals along the cold-bore, serve only to pump He from possible leaks and H_2 stemming from end effects at warm-to-cold transitions. These pumps, operating at $\sim 10^{o}$K, have $\sim 10^{3}$ greater capacity for He than sputter-ion pumps,[12] and they are easily regenerated. Gold beam lifetime and emittance growth are shown to be severely impacted by increases in the partial pressures of H_2 and He in the cold-bore.[13] This is illustrated

in Fig. 10 where beam lifetimes are given for various size 4.2°K He leaks with and without the use of sorption pumps.[14]

The interconnects of the magnet cryostats are joined with a welded, split "clamshell". Further, no "hard" vacuum barriers are used to segment each of the twelve, 480 m cryostats. This presents some rather unique challenges in terms of locating and remedying He leaks from the magnets into the cryostat vacuum system. The probability is greatest that a He leak will occur in the region where the magnets are interconneted. Ergo, one must be able to locate a He leak with a longitudinal resolution finer than the shortest magnet in a magnet string. Toward this end, three turbomolecular pumps are positioned along each 480 m cryostat (i.e., see Fig. 8). One purpose of these pumps is to create a He gradient along a cryostat in the event of a He leak from a magnet interconnect into the cryostat. The quadrupole residual gas analyzers positioned along the cryostat serve to "point" in the approximate direction of the He leak. Transverse conduits, thermally baffled, couple each 4.2°K interconnect region to valves located on the magnet cryostat at each magnet interconnect. A leak detector may be used to successively measure He pressure at each interconnect until the interconnect with the maximum He pressure is located (i.e., the offending interconnect). An example of this technique is shown in Fig. 11, when proof of principle was established with a contrived leak on a RHIC full cell test. The transverse conduits must also have sufficient conductance to the cryostat valves to facilitate sufficient pumping on the leaks - that is, vs. longitudinal conductances along the magnets - to maintain machine operation until the leaks are repaired.

Lacking beam components such as kickers, septa and rf cavities, the RHIC warm-bore systems would be rather mundane. Sputter-ion pumps, perhaps augmented with lumped nonevaporable getters would provide the speed needed at low 10^{-10} Torr to more than adequately meet the pressure requirement.[15] However, calculations show that beam life time and emittance growth, related to warm-bore pressure, will be deleteriously impacted by beam components, in particular rf cavities. Further, H_2 stemming from these cavities, and finding its way into the

cold-bore system would prove a problem absent the use of sorption pumps. For this reason, sputter-ion pumps will be augmented with titanium sublimation pumps in the RHIC warm-bore systems.

The instrumentation and control system features use of multidrop RS-485 data bus through which instrumentation controllers report to eight programmable logical controllers (PLCs) distributed in radiation-free areas about the complex. Gauges and instrumentation controllers will be located within the RHIC ring except in high radiation areas. We presently plan to use Bayard-Alpert gauges to measure pressure in the cold-bore and warm-bore regions, and cold cathode gauges to measure pressure in the cryostats. For purposes of software commonality and component cost reduction we are exploring the possible use of inverted magnetron gauges in all RHIC HV and UHV applications. In UHV applications, gauge ignition will be enhanced through use of either Co^{60} or Ni^{63} radioactive sources.[16]

5. Summary

The vacuum systems of three machines at AGS-RHIC facility have been described with emphasis on the development in a few areas, such as the noise pickup in the vacuum monitoring of the Booster ultrahigh vacuum system; the development of the distributed ion pumps for muon storage ring and the locating of helium leaks in the 480 m long RHIC cryostats. The present results are applicable to other accelerators and storage rings such as CERN's Large Hadron Collider.

6. Acknowledgments

The authors gratefully appreciate the support of Dr. S. Ozaki, Head of the RHIC Project, Dr. D.I. Lowenstein, AGS Department Chairman, our colleagues, and the U.S. Department of Energy for their continuing support in this work.

7. References

[1]W.T. Weng, 1993 IEEE Particle Accel. Conf. Proc., **5**, 3726 (1993).

[2]V.W. Hughes and G. zu Putlitz, Quantum Electrodynamics, p. 802, World Scientific, Singapore (1990).

[3]S. Ozaki, 1991 IEEE Particle Accel. Conf. Proc., **5**, 2901 (1991).

[4]H.C. Hseuh, et.al., J. Vac. Sci. Technol., **A10**, 2085 (1992).

[5]J. Gabusi, et al., Vacuum, **44**, 527 (1993).

[6]H.C. Hseuh, et.al., 1989 IEEE Particle Accel. Conf. Proc., **1**, 574 (1989).

[7]H.C. Hseuh, M. Mapes and L. Snydstrup, 1993 IEEE Particle Accel. Conf. Proc., **5**, 3897 (1993).

[8]Y. Suetsugu and M. Nakagawa, Vacuum, **42**, 761 (1991).

[9]H. Hartwig and J.S. Kouptsidis, J. Vac. Sci. Technol., **11**, 1154 (1974).

[10]H.C. Hseuh, W.S. Jiang and M. Mapes, J. Vac. Sci. Technol., **A12**, (1994) (in press).

[11]K.M. Welch, Stanford Linear Accel. Center Tech. Note SLAC-TN-72-10, July 1972 (unpublished).

[12]K.M. Welch, D.J. Pate and R.J. Todd, J. Vac. Sci. Technol., **A11**, 1607 (1993).

[13]M. Rhodes-Brown and M. Harrison, BNL-47070 Informal Report, Dec. 1991 (unpublished).

[14]J.P.Hobson and K.M. Welch, J. Vac. Sci. Technol., **A11**, 1566 (1993).

[15]K.M. Welch, D.J. Pate and R.J. Todd, J. Vac. Sci. Technol., **A12**, 861 (1994).

[16]C. Hayashi, J. Vac. Sci. Technol., **3**, 286 (1966).

Figure Captions

Fig. 1. Brookhaven's AGS-RHIC facility.

Fig. 2. The normalized intensity of Au^{+33} beam during the Booster acceleration cycle at vacuum levels of $\sim 1x10^{-9}$ Torr and $\sim 3x10^{-11}$ Torr.

Fig. 3. The noise pickup of two Booster gauge cables with E4 gauge having outdoor cable length of 150 m and B7 gauge of 70 m.

Fig. 4. The pumping speeds of ion pump elements of different cell size versus the magnetic field.

Fig. 5. The decrease in pumping speeds versus alignment angle(angle between the direction of magnetic field and the anode axis.

Fig. 6. The discharge intensity of a Penning cold cathode gauge vs magnetic field at different alignment angle.

Fig. 7. The layout of the Relativistic Heavy Ion Collider.

Fig. 8. Vacuum instrumentation and pumping for a 12th of the RHIC machine.

Fig. 9. Cryostat and ultrahigh vacuum interconnect hardware.

Fig. 10. Average pressure and gold beam lifetimes in one RHIC ring due to one helium leak of magnitude 10^{-n} Torr-ℓ/sec in the 6.9 cm diameter beam tube.

Fig. 11. Helium pressure profile in magnet string due to introducing contrived leaks with the magnets at temperatures of ~ 4.4 and 293 K.

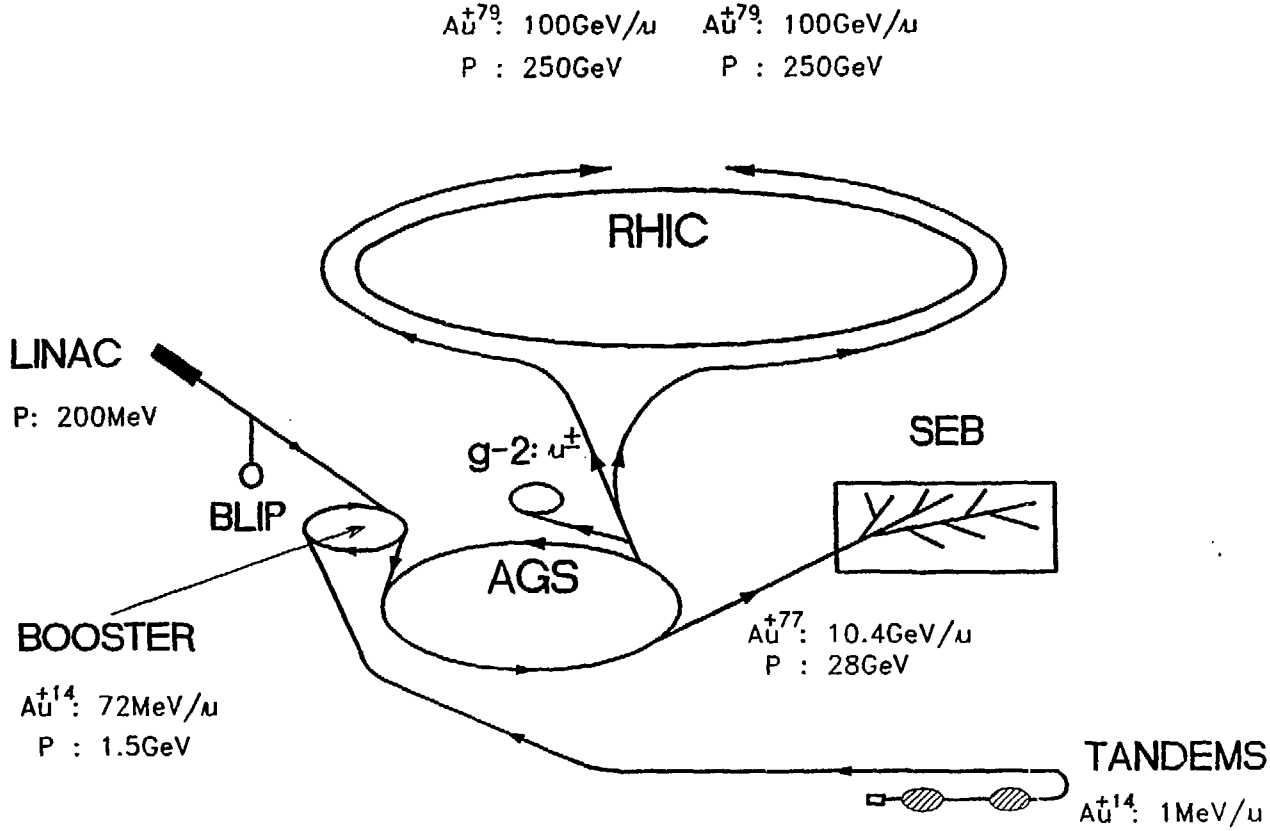

AGS-RHIC Complex

Figure 1

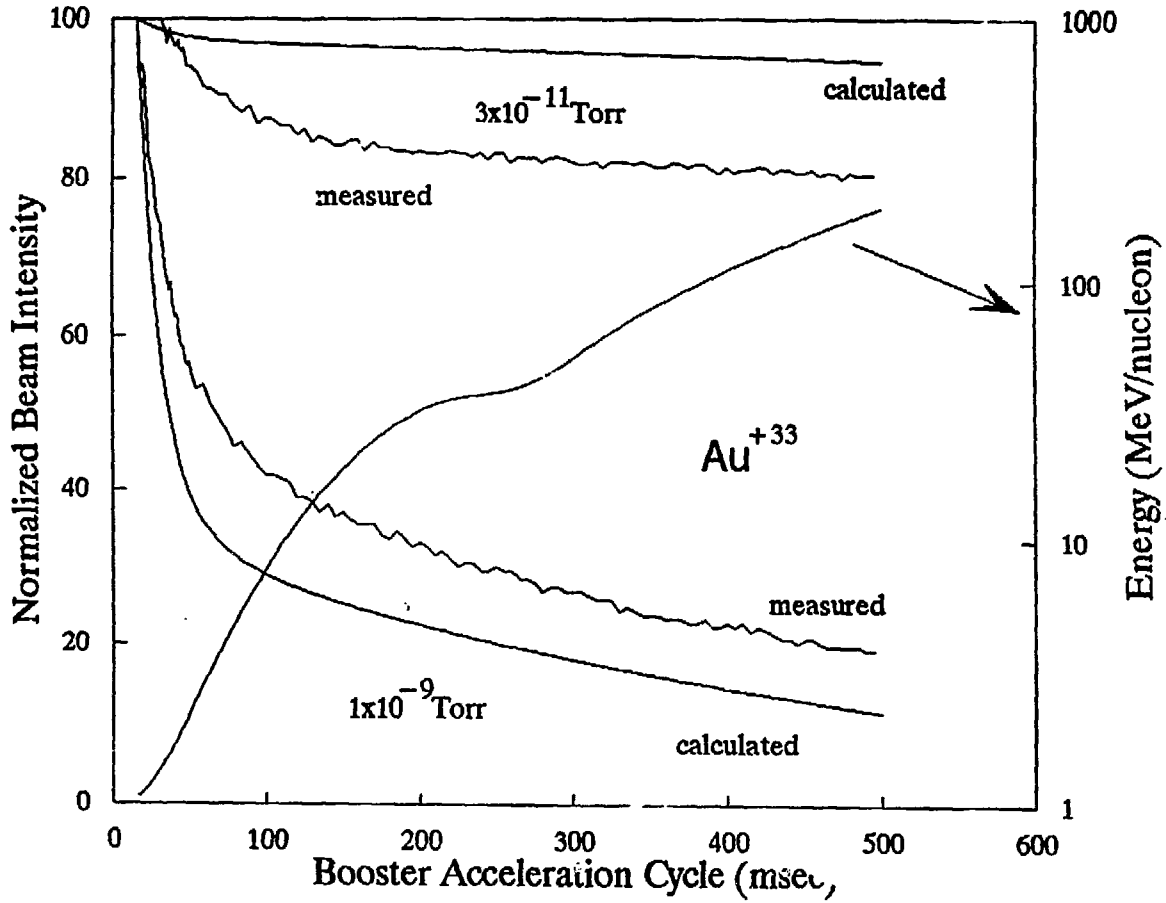
100
80
60
40
20
0
Normalized Beam Intensity
1000
100
10
1
Energy (MeV/nucleon)
0
100
200
300
400
500
600
Booster Acceleration Cycle (msec)
calculated
3x10^{-11}Torr
measured
Au^{+33}
measured
1x10^{-9}Torr
calculated

Figure 2

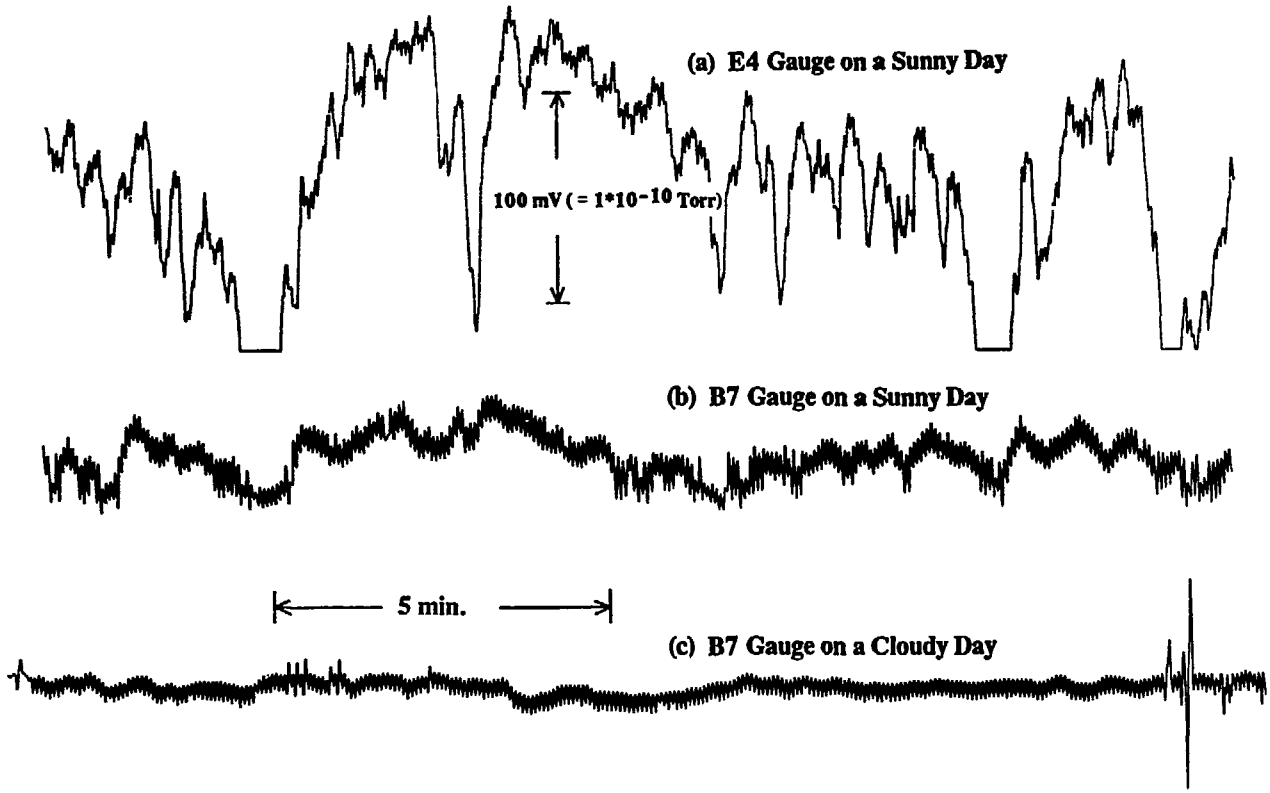
(a) E4 Gauge on a Sunny Day
100 mV (= 1*10-10 Torr)
(b) B7 Gauge on a Sunny Day
5 min.
(c) B7 Gauge on a Cloudy Day

Figure 3

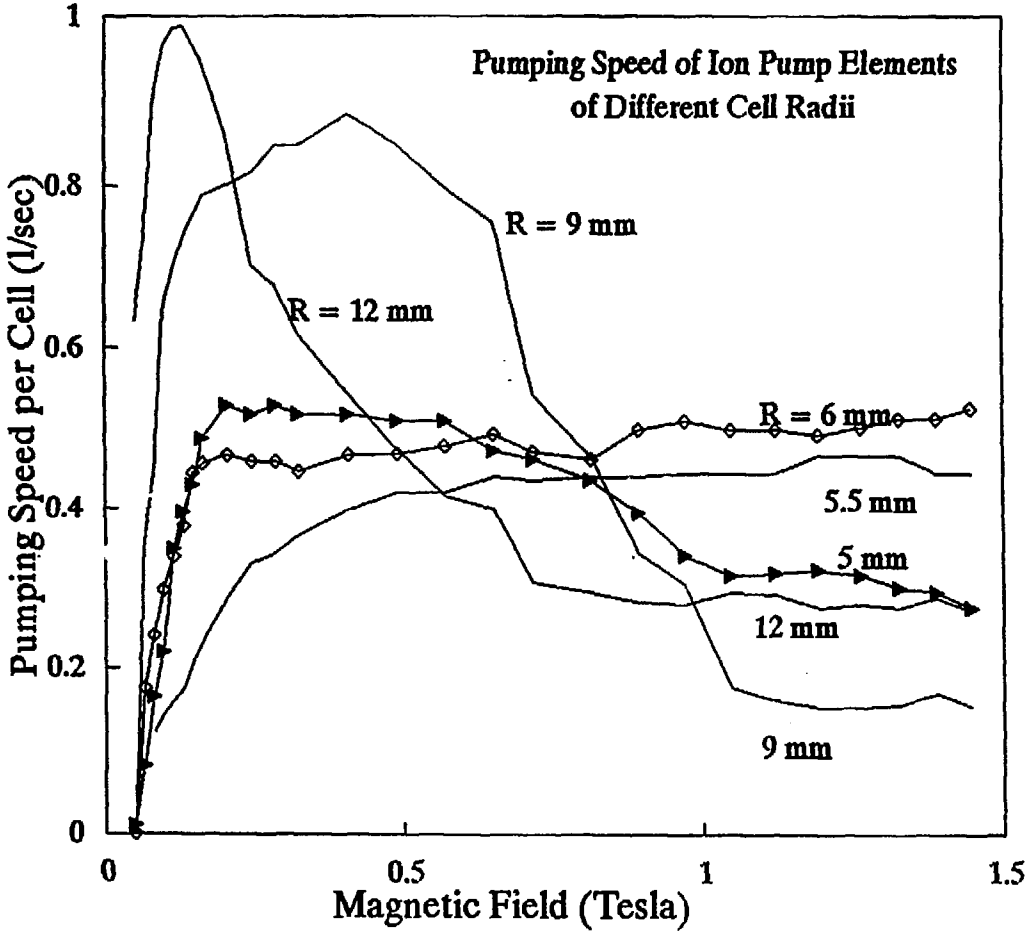
Pumping Speed of Ion Pump Elements
of Different Cell Radii
R = 9 mm
R = 12 mm
R = 6 mm
5.5 mm
5 mm
12 mm
9 mm
Pumping Speed per Cell (l/sec)
Magnetic Field (Tesla)
0
0.2
0.4
0.6
0.8
1
0
0.5
1
1.5

Figure 4

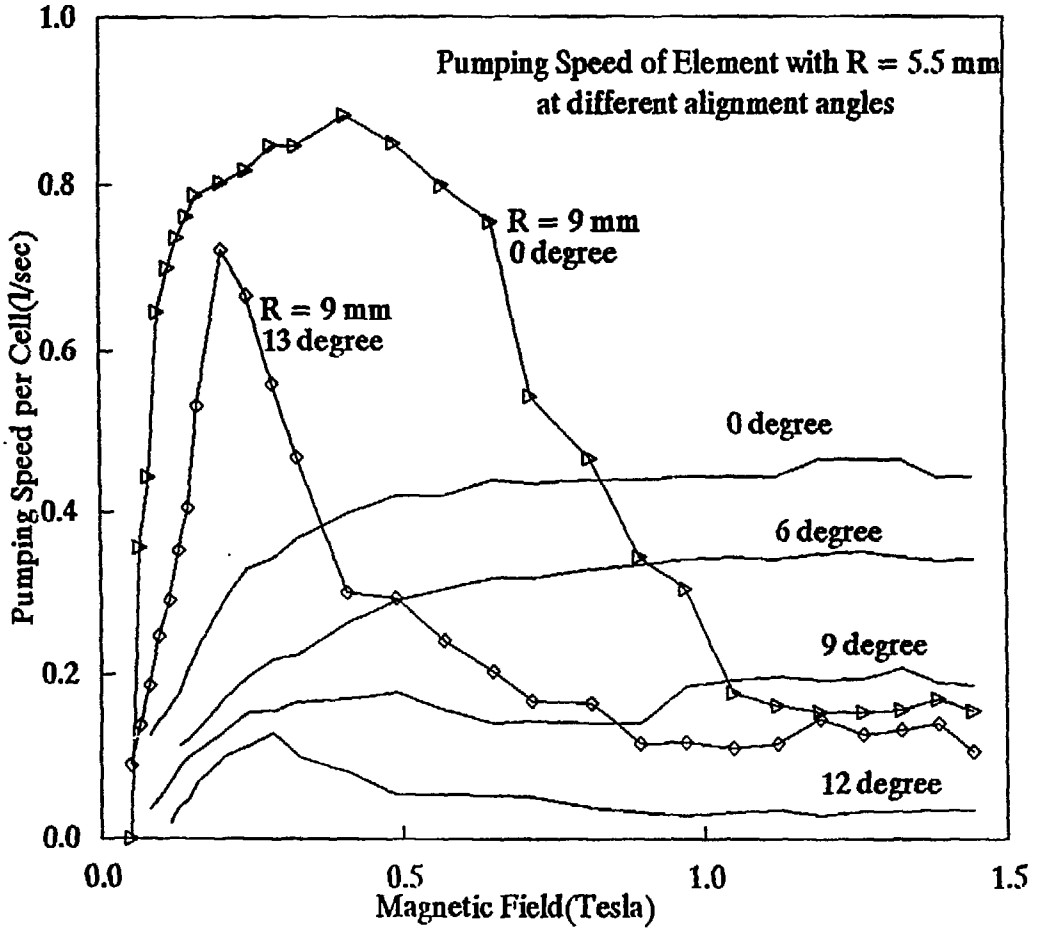
Pumping Speed of Element with R = 5.5 mm
at different alignment angles
R = 9 mm
0 degree
R = 9 mm
13 degree
0 degree
6 degree
9 degree
12 degree
Pumping Speed per Cell(l/sec)
Magnetic Field(Tesla)
1.0
0.8
0.6
0.4
0.2
0.0
0.0
0.5
1.0
1.5

Figure 5

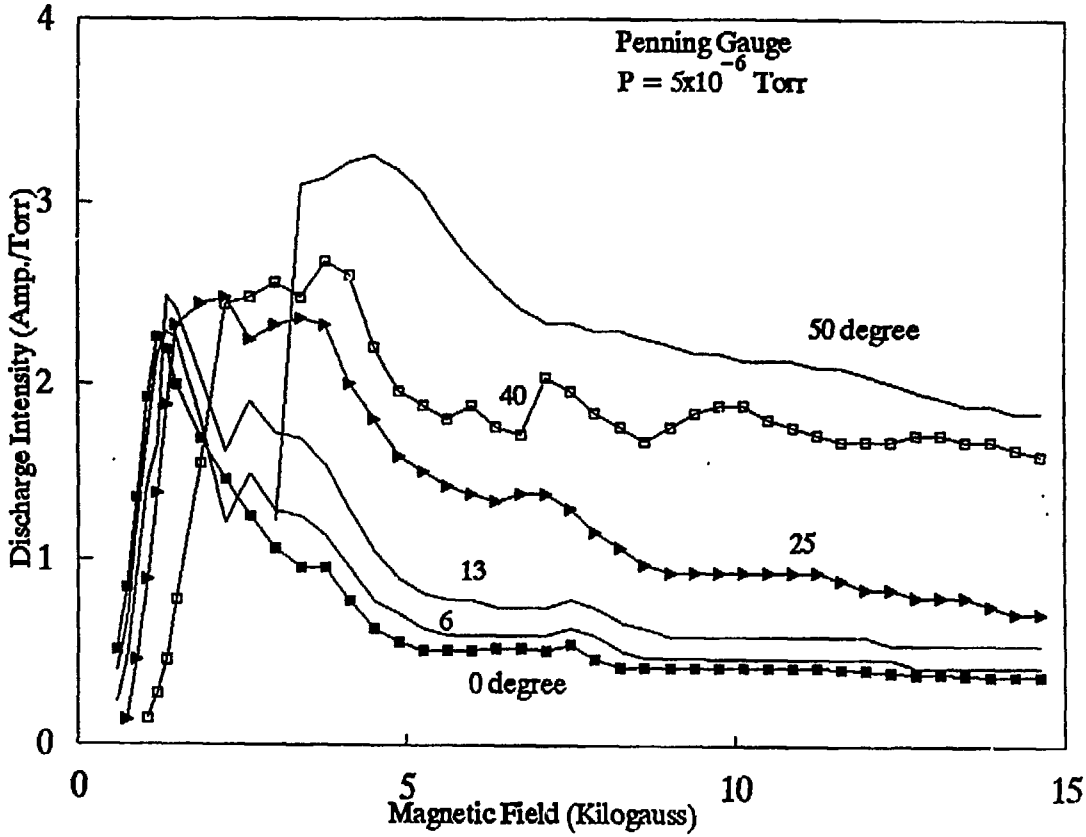
Penning Gauge
P = 5x10^-6 Torr
Discharge Intensity (Amp./Torr)
Magnetic Field (Kilogauss)
50 degree
40
25
13
6
0 degree
0
1
2
3
4
0
5
10
15

Figure 6

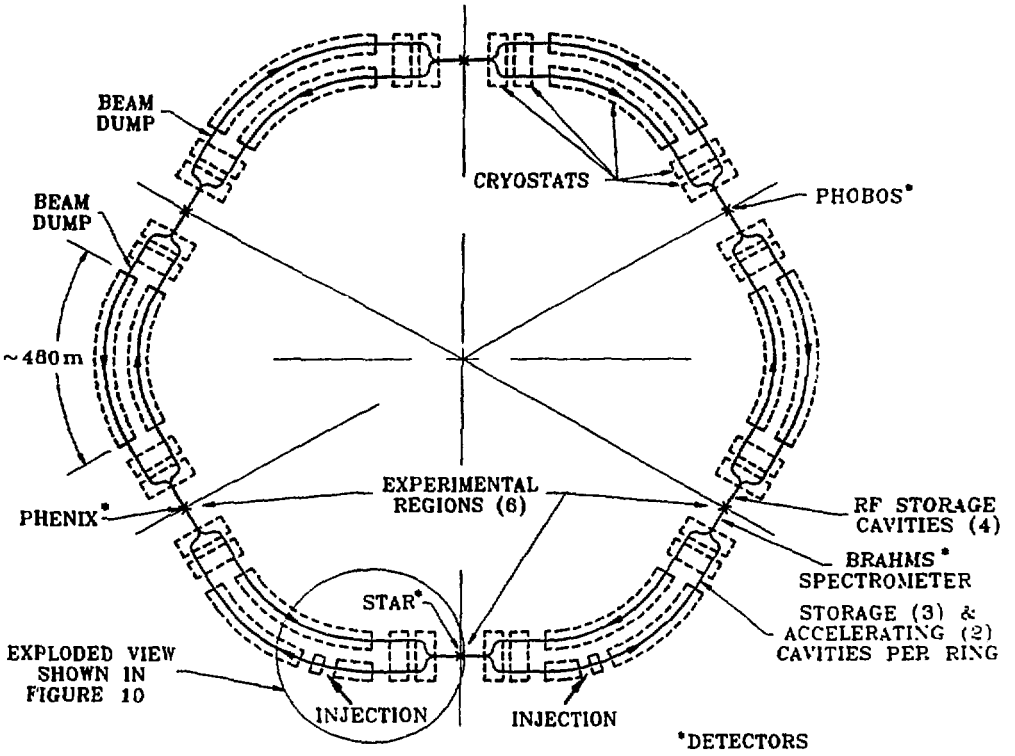
BEAM DUMP
BEAM DUMP
~480m
CRYOSTATS
PHOBOS*
EXPERIMENTAL REGIONS (6)
PHENIX*
RF STORAGE CAVITIES (4)
BRAHMS* SPECTROMETER
STAR*
STORAGE (3) & ACCELERATING (2) CAVITIES PER RING
EXPLODED VIEW SHOWN IN FIGURE 10
INJECTION
INJECTION
*DETECTORS

Figure 7

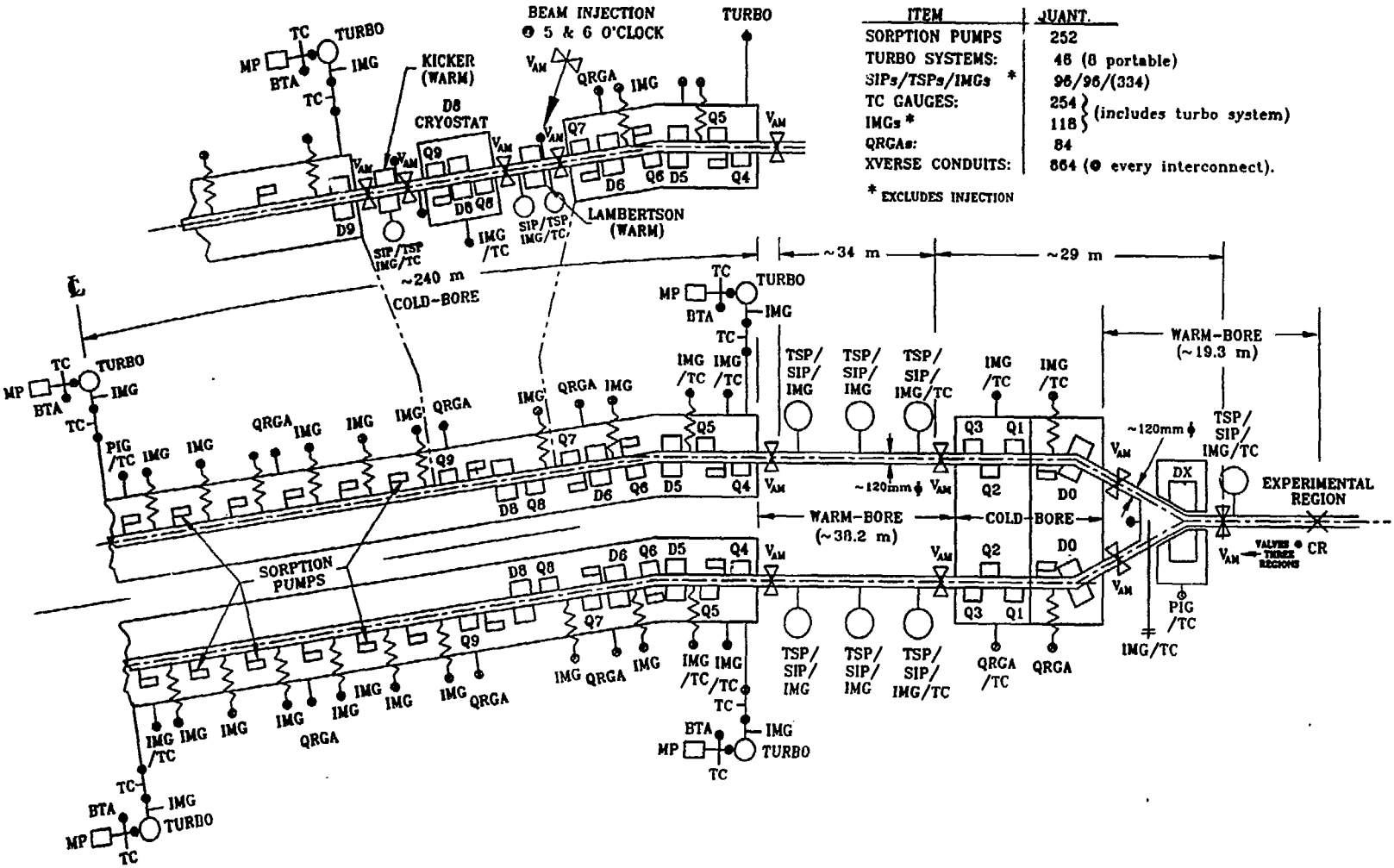

ITEM	QUANT.
SORPTION PUMPS	252
TURBO SYSTEMS:	46 (8 portable)
SIPs/TSPs/IMGs *	96/96/(334)
TC GAUGES:	254 } (includes turbo system)
IMGs *	118 }
QRGAs:	84
XVERSE CONDUITS:	864 (@ every interconnect).

* EXCLUDES INJECTION

Figure 8

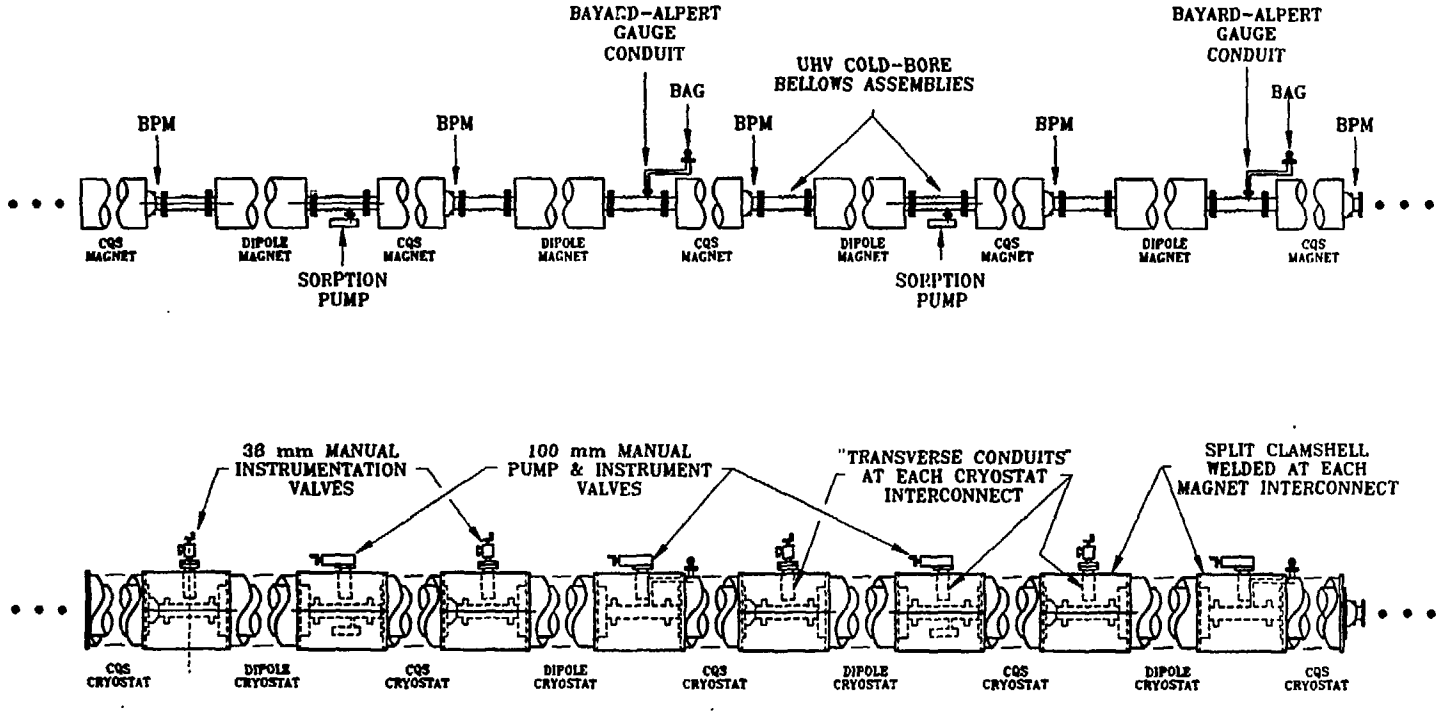
BAYARD-ALPERT GAUGE CONDUIT
BAG
UHV COLD-BORE BELLOWS ASSEMBLIES
BAYARD-ALPERT GAUGE CONDUIT
BAG
BPM
BPM
BPM
BPM
BPM
CQS MAGNET
DIPOLE MAGNET
CQS MAGNET
DIPOLE MAGNET
CQS MAGNET
DIPOLE MAGNET
CQS MAGNET
DIPOLE MAGNET
CQS MAGNET
SORPTION PUMP
SORPTION PUMP
38 mm MANUAL INSTRUMENTATION VALVES
100 mm MANUAL PUMP & INSTRUMENT VALVES
"TRANSVERSE CONDUITS" AT EACH CRYOSTAT INTERCONNECT
SPLIT CLAMSHELL WELDED AT EACH MAGNET INTERCONNECT
CQS CRYOSTAT
DIPOLE CRYOSTAT
CQS CRYOSTAT
DIPOLE CRYOSTAT
CQS CRYOSTAT
DIPOLE CRYOSTAT
CQS CRYOSTAT
DIPOLE CRYOSTAT
CQS CRYOSTAT

Figure 9

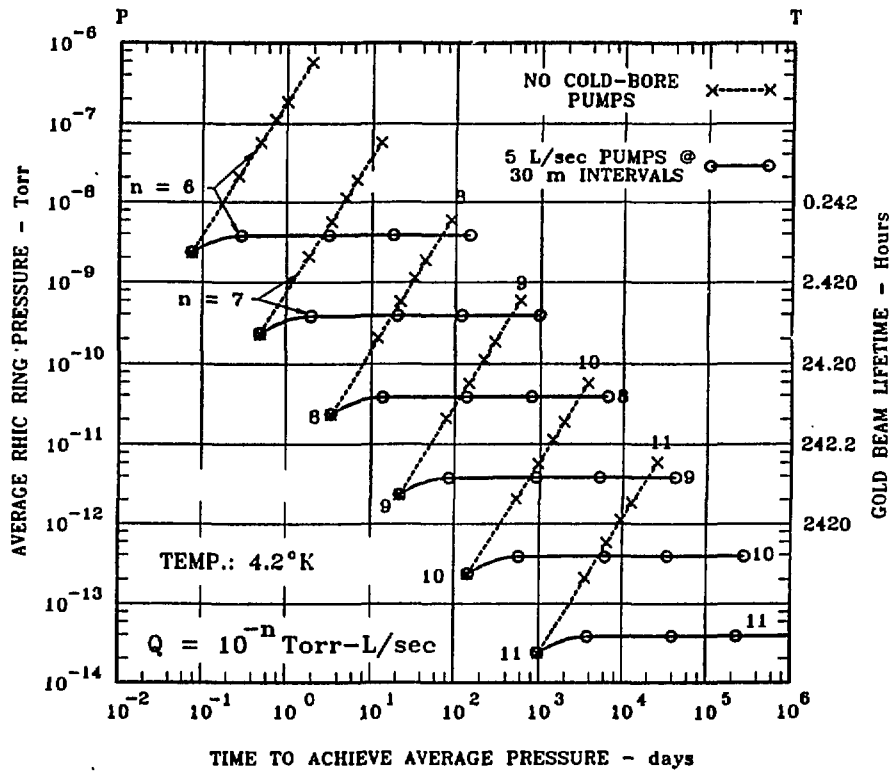
P
T
NO COLD-BORE PUMPS
5 L/sec PUMPS @ 30 m INTERVALS
n = 6
n = 7
TEMP.: 4.2°K
Q = 10^-n Torr-L/sec
AVERAGE RHIC RING PRESSURE - Torr
GOLD BEAM LIFETIME - Hours
TIME TO ACHIEVE AVERAGE PRESSURE - days
0.242
2.420
24.20
242.2
2420

Figure 10

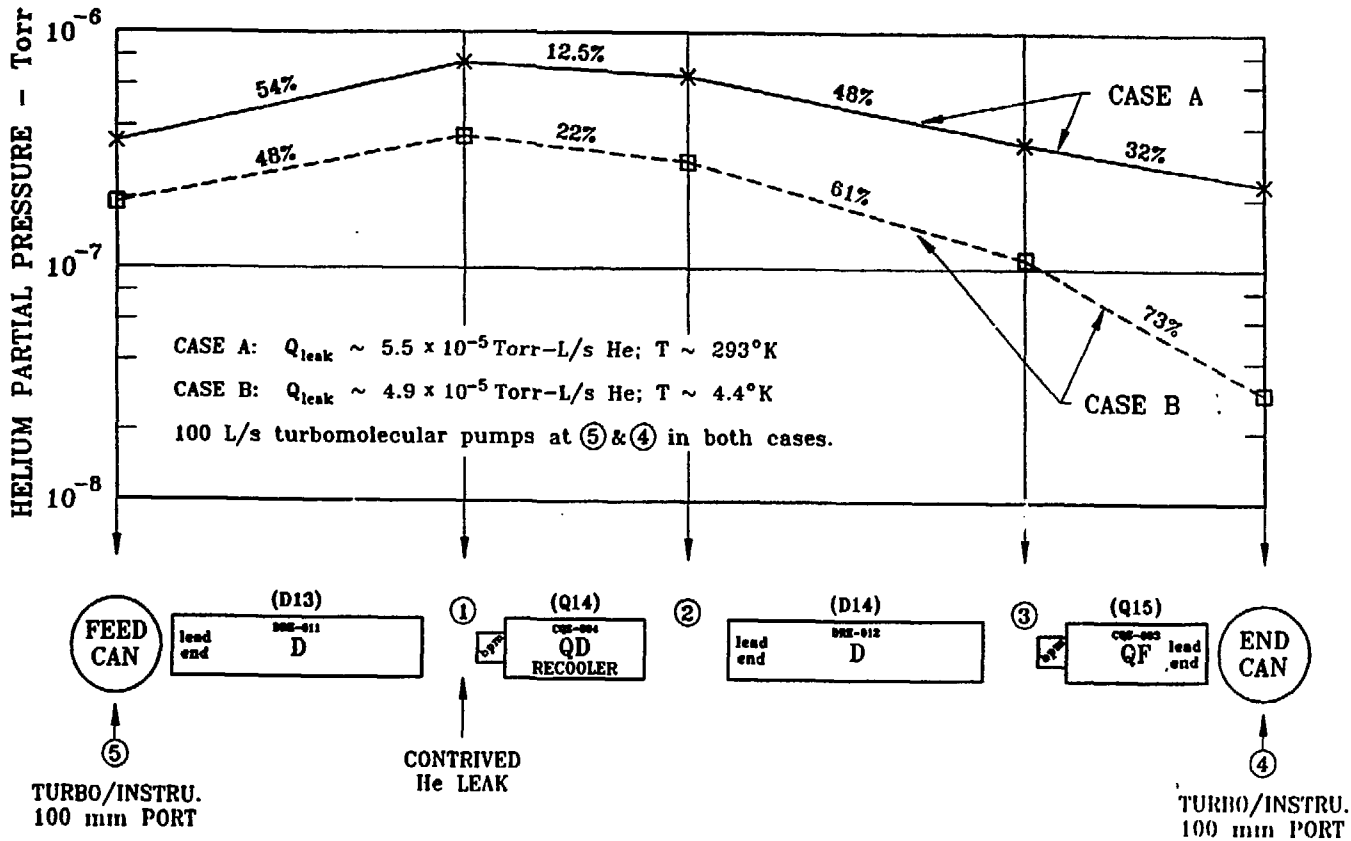
HELIUM PARTIAL PRESSURE - Torr
10^{-6}
10^{-7}
10^{-8}
54%
12.5%
48%
32%
48%
22%
61%
73%
CASE A
CASE B
CASE A: Q_{leak} ~ 5.5 x 10^{-5} Torr-L/s He; T ~ 293°K
CASE B: Q_{leak} ~ 4.9 x 10^{-5} Torr-L/s He; T ~ 4.4°K
100 L/s turbomolecular pumps at ⑤ & ④ in both cases.
FEED CAN
(D13)
lead end
D
①
(Q14)
QD
RECOOLER
②
(D14)
lead end
D
③
(Q15)
QF
lead end
END CAN
⑤
TURBO/INSTRU.
100 mm PORT
CONTRIVED
He LEAK
④
TURBO/INSTRU.
100 mm PORT

Figure 11